High Power Laser Science and Engineering, (2023), Vol. 11, e1, 6 pages.
doi:10.1017/hpl.2022.39

RESEARCH ARTICLE

High temporal contrast 1053 nm laser source based on optical parametric amplification and second-harmonic generation

Liya Shen[1,2,3], Yanyan Li[1], Wenkai Li[1], Jiajun Song[1], Junyu Qian[1,3], Jianyu Sun[1,3], Renyu Feng[1,3], Yujie Peng[1], and Yuxin Leng[1,2,3]

[1] *State Key Laboratory of High Field Laser Physics, Shanghai Institute of Optics and Fine Mechanics, Chinese Academy of Sciences, Shanghai, China*

[2] *School of Physical Science and Technology, ShanghaiTech University, Shanghai, China*

[3] *Center of Materials Science and Optoelectronics Engineering, University of Chinese Academy of Sciences, Beijing, China*

(Received 6 May 2022; revised 26 October 2022; accepted 23 November 2022)

Abstract

Temporal contrast directly affects the interaction between ultraintense and ultrashort pulse lasers with matter. Seed laser sources with broad bandwidth and high temporal contrast are significant for overall temporal contrast enhancement. The technique of cascaded nonlinear processes with optical parametric amplification and second-harmonic generation is demonstrated for high temporal contrast seed source generation. Within 40 ps before the main pulse, the temporal contrast reaches over 10^{11}. The pulse energy and duration of the high-contrast pulse are 112 μJ and 70 fs, respectively. Considering its high beam quality and stability, this laser source can serve as a high-quality seed for Nd:glass-based ultraintense and ultrashort pulse laser facilities.

Keywords: high temporal contrast; nonlinear effect; optical parametric amplification

1. Introduction

Ultraintense and ultrashort lasers can be used in high-field physics[1], laser-driven particle acceleration[2] and so on[3–6]. Nowadays, the peak power of the ultrafast laser has reached the level of 10 PW (1 PW = 10^{15} W)[7], and many ultraintense laser facilities have sprung up[8–10]. Among the gain media used in amplifiers, Nd:glass[11] has high saturation fluorescence and a long upper-state lifetime, and facilitates the fabrication of large apertures. Thanks to these merits, laser systems based on Nd:glass can deliver extremely high-energy pulses for applications such as inertial confinement fusion or proton acceleration. For most of the aforementioned applications, temporal contrast is one of the key parameters. Nowadays, the focused intensity of the laser has reached 10^{23} W/cm^2[12]. The ionization threshold of the solid targets ranges from 10^{10} to 10^{12} W/cm^2. However, conventional commercial lasers have a temporal contrast of 10^6–10^7 or worse, so the pre and pedestal pulses may cause target pre-ionization and affect the interaction between the main pulse and the targets.

To suppress the pre and pedestal pulses, many methods have been proposed, such as plasma mirrors[13,14] after compression, second-harmonic generation (SHG)[15], cross-polarized wave (XPW)[16–18], nonlinear elliptic polarization rotation (NER)[19,20], and optical parametric amplification (OPA)[21]. However, energy loss induced by plasma mirrors cannot be compensated by further amplification. Although XPW and NER are simple and can broaden the spectrum, wavelength shift or tuning is difficult, and it may cause optical element damage with higher energy. OPA has the characteristic of wavelength tuning and can significantly enhance temporal contrast related to its high gain factor[21].

Both OPA and SHG can enhance the temporal contrast and tune the wavelength. In this paper, we demonstrate the combination of cascaded OPA and SHG processes to obtain seed pulses with broad bandwidth and high temporal contrast. In our experiment, an Yb-doped femtosecond laser is used as the driven source. The output 1053 nm pulse energy and duration are 112 μJ and 70 fs, respectively. The measured temporal contrast exceeds 10^{11}, which is limited by the dynamic range of the measurement equipment.

Correspondence to: Yanyan Li, Yujie Peng, and Yuxin Leng, State Key Laboratory of High Field Laser Physics, Shanghai Institute of Optics and Fine Mechanics, Chinese Academy of Sciences, Shanghai 201800, China. Email: yyli@siom.ac.cn (Y. Li); yjpeng@siom.ac.cn (Y. Peng); lengyuxin@siom.ac.cn (Y. Leng)

As a seed source, the beam stability and quality are adequate. Compared to other works driven by 800 nm laser[22,23], parasitic third-order nonlinear effects can be reduced because of the scaling of the critical power for self-focusing with λ^2[24]. Despite the narrow bandwidth of the Yb laser, spectral broadening and wavelength tuning can be achieved by OPA.

2. Experimental setup

The scheme of the high temporal contrast 1053 nm laser source is demonstrated in Figure 1(a). A commercial laser source (Pharos, Light Conversion) is used as the driving laser, delivering a pulse energy of 2 mJ at a repetition rate of 1 kHz. The central wavelength and the pulse duration are 1036.8 nm and 180 fs, respectively. The apparatus mainly consists of the white-light generation (WLG) process, OPA process, and SHG process.

The driving laser pulse is divided into three parts with two polarization beam splitters (PBSs) and half-wave plates (HWPs), and the energy can be adjusted precisely. The fraction of the reflected part of PBS2 is used for WLG. Through an aperture and a neutral density filter, the pulse energy and diameter are controlled to a proper level to generate a stable single filament. For long wavelength pulses (such as 1036 nm), low-bandgap materials such as yttrium aluminum garnet (YAG) outperform sapphire for WLG[25,26]. With one 4-mm-thick YAG crystal, the generated white light has a broad spectral coverage from about 350 to 2200 nm (inset red area in Figure 2(a)), and the signal pulse of NOPA1 (noncollinear OPA) is part of it (Figure 2(a) inset blue line). The transmitted part (~90 μJ) of PBS2 is used as the pump pulse for NOPA1. Here, we utilize a noncollinear structure because a collinear structure, which is constrained by optical coatings, may make it impossible to distinguish between the signal and the idler pulses. The noncollinear angle is less than 0.7°. With lenses L4 (f = 150 mm) and L5 (f = 250 mm), the signal and pump pulses are focused on the nonlinear crystal 1 (beta barium borate (β-BBO), type II phase-matching, 8 mm × 8 mm × 4 mm, θ = 29.7°, ϕ = 30°). To avoid damage to the crystal and ensure pump intensity, the focal spot of the pump pulse is close to the crystal. By precise control of the spatial overlap and the time delay between the signal pulse and the pump pulse, the most efficient amplification can be achieved, and the energy of the amplified signal pulse is about 1 μJ. The pump intensity I_p = 149 GW/cm^2 and the corresponding small signal gain is 2.98 × 10^6. Then the amplified pulse is collimated by L6 (f = 200 mm) and amplified in NOPA2. The reflection part (about 1.87 mJ) of PBS1 is used as the pump pulse for NOPA2, which is collimated by L1 (f = 200 mm) and L2 (f = –100 mm) to match the size of the signal pulse. Both beam sizes are 3.2 mm in diameter. At this stage, the pump intensity I_p = 116 GW/cm^2 and the small signal gain is 7.8 × 10^7. Similar to NOPA1, the noncollinear angle of NOPA2 is also less than 0.7° to reduce the negative influence of the angular chirp of the idler pulse. Figure 1(b) displays the details of the NOPA. With accurate spatial and temporal overlap, an amplified signal pulse and a generated idler pulse can be achieved. By slightly adjusting nonlinear crystal 2 (β-BBO, type I phase-matching, 8 mm × 8 mm × 3 mm, θ = 21.3°, ϕ = 0°), the central wavelength of the output pulses can be tuned. In this experiment, the center wavelength is set at 2106 nm. With one type I phase-matching BBO crystal (θ = 21°, ϕ = 0°, 10 mm × 10 mm × 0.8 mm),

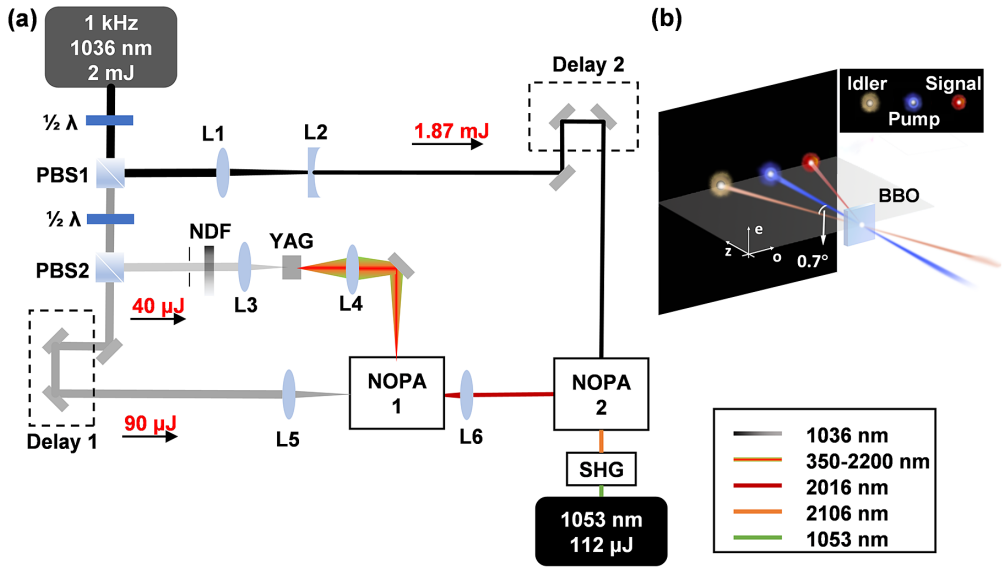

Figure 1. (a) Scheme of the 1053 nm laser source. PBS: polarization beam splitter; L: lens; NDF: neutral density filter; NOPA: noncollinear OPA. The linewidth indicates the beam size roughly and the shade indicates the pulse energy. (b) Schematic of the NOPA, where the angle between the signal and the pump is less than 0.7°.

https://doi.org/10.1017/hpl.2022.39 Published online by Cambridge University Press

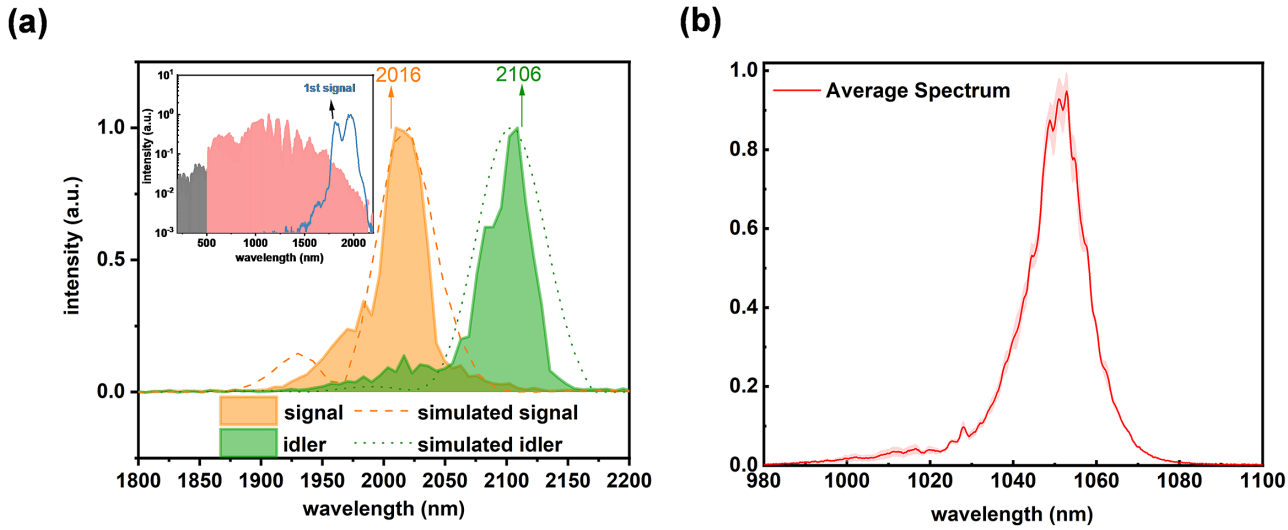

Figure 2. (a) Spectra of NOPA2 output. The orange area is the amplified signal pulse and the green area is the idler pulse of NOPA2. The orange dashed line (simulated signal) and green dotted line (simulated idler) are the simulated spectra. The red area of the inset is the spectrum of the white light generated by YAG, and the jitter before 500 nm (gray area) may be caused by stray light of the spectrometer. The blue line of the inset is the amplified signal pulse of NOPA1. (b) Spectra of second-harmonic generation of the idler from NOPA2. The spectra fluctuate in the red area, and the middle solid line is the average value.

we achieved SHG at 1053 nm, and the 1053 nm pulses are separated from the 2106 nm pulses with two dichroic mirrors.

3. Results and discussion

Based on the NOPA and SHG processes, the center wavelength is successfully transferred from 1036 to 1053 nm. With nearly degenerate OPA, the achieved amplified pulse has an energy of 246 μJ and a central wavelength of 2106 nm (Figure 2(a), green area). A theoretical model[27] based on the coupled second-order three-wave nonlinear propagation equations in the plane-wave limit is used to simulate the OPA progress (Figure 2(a), orange dashed and green dotted lines). The center wavelength is tuned to 2106 nm to gain the optimum double-frequency efficiency. After the SHG

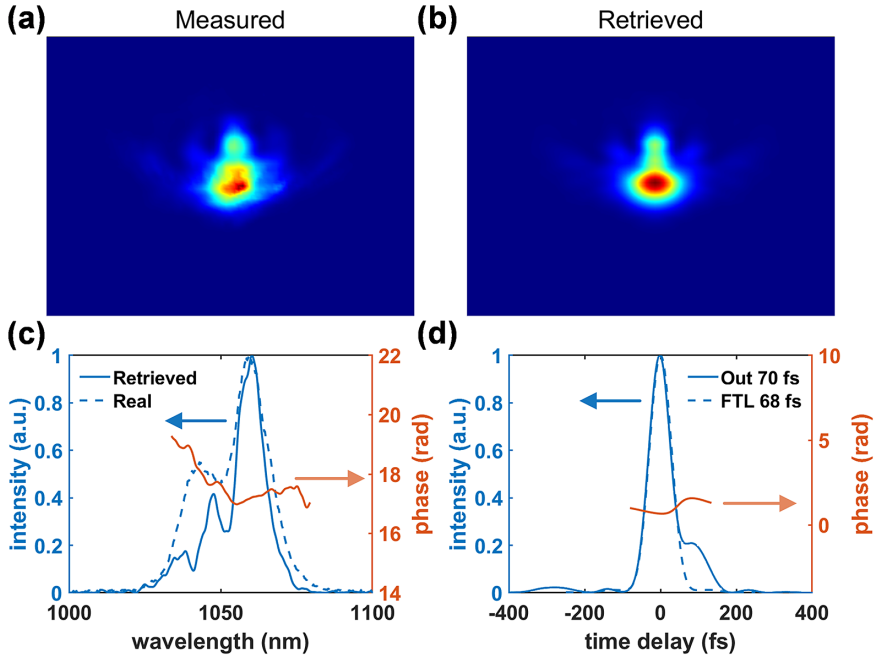

Figure 3. Pulse width of the output 1053 nm. (a) Measured FROG trace. (b) Retrieved FROG trace. (c) Retrieved spectral intensity (blue solid line), spectral phase (orange), and actual spectrum of 1053 nm (blue dashed line). (d) Retrieved temporal intensity (blue solid line), retrieved temporal phase (orange) and Fourier transform-limited pulse (blue dashed line). The grid sizes are 256 × 256.

https://doi.org/10.1017/hpl.2022.39 Published online by Cambridge University Press

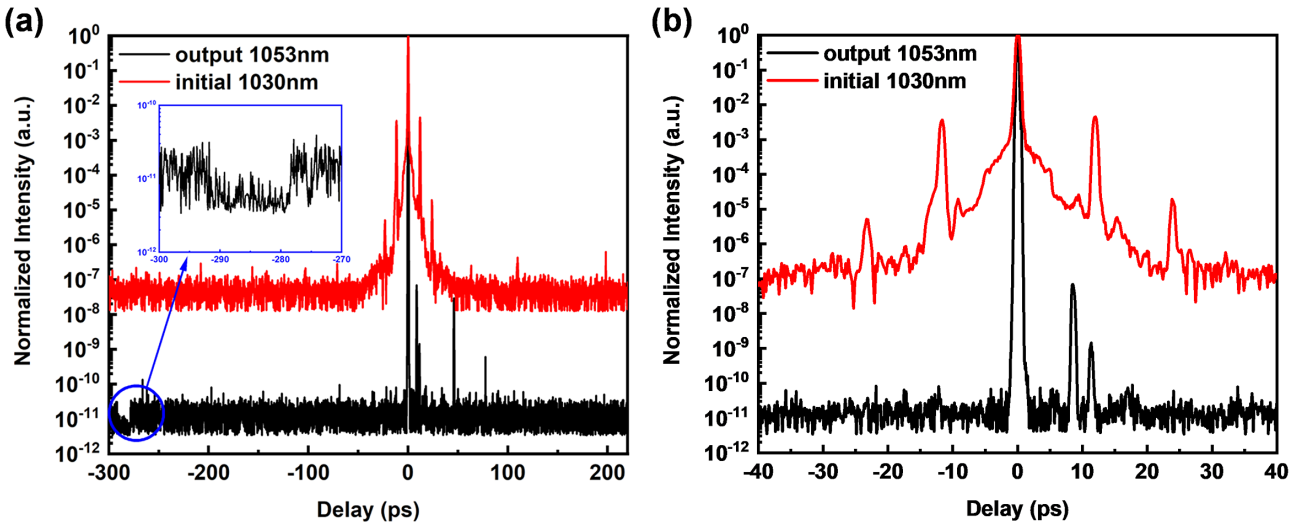

Figure 4. (a) Temporal contrast of the initial 1030 nm (red line) and output 1053 nm (black line) pulses. The blue box indicates the noise level. (b) Details of the temporal contrast of the initial 1030 nm (red line) and output 1053 nm laser pulses (black line) at ±40 ps time.

process, the energy of the output 1053 nm pulse is 112 μJ and the spectrum is as shown by the red solid line in Figure 2(b). According to the SHG efficiency $\eta = \left(\frac{5.46\, d_{\text{eff}}}{\lambda_0 n_0^{\frac{3}{2}}}\right)^2 \times L^2 \times I_{\lambda_0} \times \text{sinc}^2\left(\frac{\Delta kL}{2}\right)$ and the phase-matching bandwidth $\lambda_{\text{FWHM}} = \frac{0.44\,\lambda_0/L}{\left|n'(\lambda_0) - \frac{1}{2}n'(\lambda_0/2)\right|}$, the trade-off between efficiency and spectral width should be considered. Therefore, 0.8 mm BBO is chosen to gain a broad enough bandwidth at optimized efficiency. The spectral stability is measured over 60 min, containing 3600 spectra (Ocean Optics). Each spectrum is the integrated spectra of 100 pulses because the integral time is 100 ms. As shown in Figure 2(b), the spectral jitter range (red area) is very small, which guarantees stable operation of the laser in the future. Because the pump and signal pulses originate from the same driving laser, the idler is passively carrier envelop phase (CEP) stable[28]. The CEP of the second harmonic is related to the fundamental pulses. As

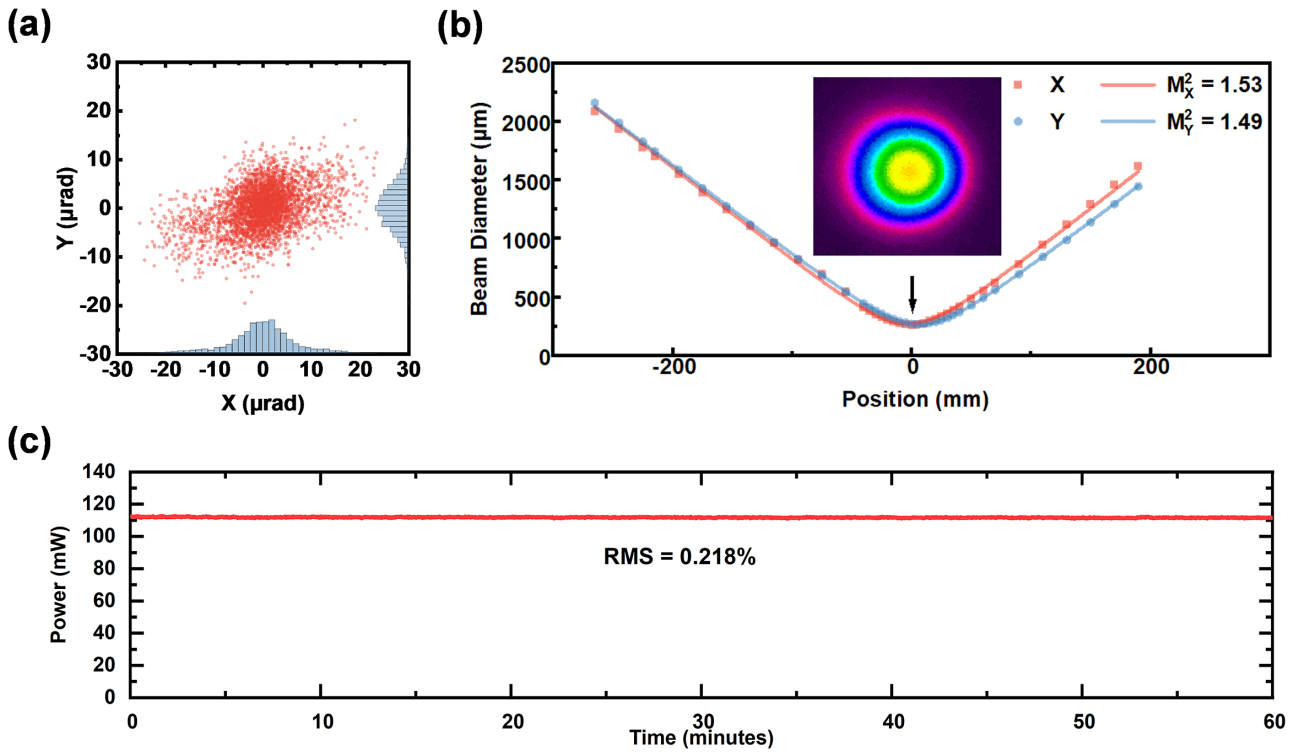

Figure 5. The quality of the output 1053 nm beam. (a) The beam pointing stability. (b) The M^2 quality of the output laser beam. (c) The power stability.

https://doi.org/10.1017/hpl.2022.39 Published online by Cambridge University Press

a result, the generated 1053 nm pulse is also passively CEP stabilized.

The pulse duration of the output 1053 nm pulse is measured by the frequency-resolved optical gating method (FROG, GRENOUILE, Swamp Optics). Compensated by chirped mirrors (UltraFast Innovations, –2400 fs^2, 950–1120 nm), the pulse duration is compressed to 70 fs (Figure 3). The reconstruction error of FROG is about 0.8%. The calculated Fourier transform limited (FTL) duration is 68 fs, implying that the focusing in the NOPA does not introduce disastrous high-order dispersion.

The temporal contrast of the seed laser is key in high-field laser physics, and we measured it by a third-order autocorrelator (Sequoia 1000, Amplitude Technologies), as shown in Figure 4. The pedestal is eliminated and the prepulses or postpulses are weakened individually. The dynamic range of the measurement device limits the observed contrast, as shown in the Figure 4(a) inset, which denotes the noise level. Within 40 ps before the main pulse, the temporal contrast has reached 10^{11}. Subsequent amplification in the main amplifier can be used to verify the high temporal contrast.

The stability of beam pointing and power are measured. For angular beam pointing, the output 1053 nm pulse is focused by a lens (f = 1000 mm). The beam position at the focal spot is recorded every second within 60 min (DataRay). The root-mean-square (RMS) error in the X-direction is 12.78 μrad, and the RMS error in the Y-direction is 8.54 μrad (Figure 5(a)). The power (Gentec-EO) is 112 mW for 60 min (Figure 5(b)) with an error of 0.218% (RMS), whereas the power fluctuation of the initial 1030 nm is 0.19% (RMS). Despite the NOPA scheme, the beam quality is quite good. The M^2 values (BeamSquared, Ophir) in the horizontal and vertical directions are 1.53 and 1.49, respectively (Figure 5(c)).

4. Conclusion

In summary, a high temporal contrast seed source running at 1053 nm central wavelength and a 1 kHz repetition rate has been demonstrated. Combined with OPA and SHG processes, the temporal contrast reached 10^{11} within 40 ps before the main pulse. The output power is 112 mW with stability of 0.218% RMS. Compared with the initial 1036 nm, the spectrum has been broadened by OPA, and the pulse can be compressed to 70 fs. This 1053 nm laser has excellent beam quality and stability and is a suitable seed for Nd-based ultraintense laser facilities.

Acknowledgements

This work was supported by the National Key R&D Program of China (2017YFE0123700); the Strategic Priority Research Program of the Chinese Academy of Sciences (XDB1603); the National Natural Science Foundation of China (61925507, 62075227, 12004402); the Program of Shanghai Academic/Technology Research Leader (18XD1404200); the Shanghai Municipal Science and Technology Major Project (2017SHZDZX02); the Youth Innovation Promotion Association CAS (2020248); the Shanghai Sailing Program (20YF1455000); and the Shanghai Rising-Star Program (21QA1410200).

References

1. M. M. Nazarov, A. V. Mitrofanov, D. A. Sidorov-Biryukov, M. V. Chaschin, P. A. Shcheglov, A. M. Zheltikov, and V. Y. Panchenko, J. Infrared Millimeter Terahertz Waves **41**, 1069 (2020).
2. J. N. Gruse, M. J. V. Streeter, C. Thornton, C. D. Armstrong, C. D. Baird, N. Bourgeois, S. Cipiccia, O. J. Finlay, C. D. Gregory, Y. Katzir, N. C. Lopes, S. P. D. Mangles, Z. Najmudin, D. Neely, L. R. Pickard, K. D. Potter, P. P. Rajeev, D. R. Rusby, C. I. D. Underwood, J. M. Warnett, M. A. Williams, J. C. Wood, C. D. Murphy, C. M. Brenner, and D. R. Symes, Nucl. Instrum. Methods Phys. Res. Sect. A **983**, 164369 (2020).
3. A. Di Piazza, C. Muller, K. Z. Hatsagortsyan, and C. H. Keitel, Rev. Mod. Phys. **84**, 1177 (2012).
4. F. Krausz and M. Ivanov, Rev. Mod. Phys. **81**, 163 (2009).
5. T. Tajima and G. Mourou, Phys. Rev. Spec. Top. Accel. Beams **5**, 031301 (2002).
6. G. Mourou and T. Tajima, Eur. Phys. J. Spec. Top. **223**, 979 (2014).
7. W. Li, Z. Gan, L. Yu, C. Wang, Y. Liu, Z. Guo, L. Xu, M. Xu, Y. Hang, Y. Xu, J. Wang, P. Huang, H. Cao, B. Yao, X. Zhang, L. Chen, Y. Tang, S. Li, X. Liu, S. Li, M. He, D. Yin, X. Liang, Y. Leng, R. Li, and Z. Xu, Opt. Lett. **43**, 5681 (2018).
8. C. N. Danson, C. Haefner, J. Bromage, T. Butcher, J. C. F. Chanteloup, E. A. Chowdhury, A. Galvanauskas, L. A. Gizzi, J. Hein, D. I. Hillier, N. W. Hopps, Y. Kato, E. A. Khazanov, R. Kodama, G. Korn, R. X. Li, Y. T. Li, J. Limpert, J. G. Ma, C. H. Nam, D. Neely, D. Papadopoulos, R. R. Penman, L. J. Qian, J. J. Rocca, A. A. Shaykin, C. W. Siders, C. Spindloe, S. Szatmari, R. M. G. M. Trines, J. Q. Zhu, P. Zhu, and J. D. Zuegel, High Power Laser Sci. Eng. **7**, e54 (2019).
9. D. N. Papadopoulos, J. P. Zou, C. Le Blanc, G. Chériaux, P. Georges, F. Druon, G. Mennerat, P. Ramirez, L. Martin, A. Fréneaux, A. Beluze, N. Lebas, P. Monot, F. Mathieu, and P. Audebert, High Power Laser Sci. Eng. **4**, e34 (2016).
10. J. D. Zuegel, S. W. Bahk, I. A. Begishev, J. Bromage, C. Dorrer, A. V. Okishev, and J. B. Oliver, in *CLEO* (Optica Publishing Group, 2014), paper JTh4L.4.
11. X. Lu, Y. Peng, Y. Li, X. Wang, X. Guo, Y. Xu, and Y. Leng, High Power Laser Sci. Eng. **4**, e43 (2016).
12. J. W. Yoon, Y. G. Kim, I. W. Choi, J. H. Sung, H. W. Lee, S. K. Lee, and C. H. Nam, Optica **8**, 630 (2021).
13. S. Inoue, K. Maeda, S. Tokita, K. Mori, K. Teramoto, M. Hashida, and S. Sakabe, Appl. Opt. **55**, 5647 (2016).
14. Y. Arikawa, S. Kojima, A. Morace, S. Sakata, T. Gawa, Y. Taguchi, Y. Abe, Z. Zhang, X. Vaisseau, S. H. Lee, K. Matsuo, S. Tosaki, M. Hata, K. Kawabata, Y. Kawakami, M. Ishida, K. Tsuji, S. Matsuo, N. Morio, T. Kawasaki, S. Tokita, Y. Nakata, T. Jitsuno, N. Miyanaga, J. Kawanaka, H. Nagatomo, A. Yogo, M. Nakai, H. Nishimura, H. Shiraga, S. Fujioka, F. Group, L. Group, H. Azechi, A. Sunahara, T. Johzaki, T. Ozaki, H. Sakagami, A. Sagisaka, K. Ogura, A. S. Pirozhkov, M. Nishikino, K. Kondo, S. Inoue, K. Teramoto, M. Hashida, and S. Sakabe, Appl. Opt. **55**, 6850 (2016).

https://doi.org/10.1017/hpl.2022.39 Published online by Cambridge University Press

15. D. Hillier, C. Danson, S. Duffield, D. Egan, S. Elsmere, M. Girling, E. Harvey, N. Hopps, M. Norman, S. Parker, P. Treadwell, D. Winter, and T. Bett, Appl. Opt. **52**, 4258 (2013).
16. L. P. Ramirez, D. N. Papadopoulos, A. Pellegrina, P. Georges, F. Druon, P. Monot, A. Ricci, A. Jullien, X. Chen, J. P. Rousseau, and R. Lopez-Martens, Opt. Express **19**, 93 (2011).
17. A. Jullien, O. Albert, F. Burgy, G. Hamoniaux, L. P. Rousseau, J. P. Chambaret, F. Auge-Rochereau, G. Cheriaux, J. Etchepare, N. Minkovski, and S. M. Saltiel, Opt. Lett. **30**, 920 (2005).
18. A. Jullien, O. Albert, G. Cheriaux, J. Etchepare, S. Kourtev, N. Minkovski, and S. M. Saltiel, J. Opt. Soc. Am. B **22**, 2635 (2005).
19. N. G. Khodakovskiy, M. P. Kalashnikov, V. Pajer, A. Blumenstein, P. Simon, M. M. Toktamis, M. Lozano, B. Mercier, Z. Cheng, T. Nagy, and R. Lopez-Martens, Laser Phys. Lett. **16**, 095001 (2019).
20. N. Smijesh, X. Zhang, P. Fischer, A. A. Muschet, R. Salh, A. Tajalli, U. Morgner, and L. Veisz, Opt. Lett. **44**, 4028 (2019).
21. Y. J. Wang and B. Lutherdavies, J. Opt. Soc. Am. B **11**, 1531 (1994).
22. Y. Y. Li, Y. S. Huang, J. Z. Wang, Y. Xu, X. M. Lu, D. Wang, Y. X. Leng, R. X. Li, and Z. Z. Xu, Laser Phys. Lett. **10**, 075403 (2013).
23. Z.-W. Shen, Z.-H. Wang, W. Zhang, H.-T. Fan, H. Teng, and Z.-Y. Wei, Chin. Phys. Lett. **31**, 014207 (2014).
24. C. Manzoni and G. Cerullo, J. Opt. **18**, 103501 (2016).
25. M. Bradler, P. Baum, and E. Riedle, Appl. Phys. B **97**, 561 (2009).
26. R. Riedel, A. Stephanides, M. J. Prandolini, B. Gronloh, B. Jungbluth, T. Mans, and F. Tavella, Opt. Lett. **39**, 1422 (2014).
27. W. K. Li, Y. Chen, Y. Y. Li, Y. Xu, X. Y. Guo, J. Lu, F. X. Wu, X. L. Wang, S. Li, and Y. X. Leng, J. Opt. Soc. Am. B **33**, 2450 (2016).
28. A. Baltuška, T. Fuji, and T. Kobayashi, Phys. Rev. Lett. **88**, 133901 (2002).

https://doi.org/10.1017/hpl.2022.39 Published online by Cambridge University Press